Modeling of the Phase Behavior in Ternary Triblock Copolymer/Water/Oil Systems

Mårten Svensson,[†] Paschalis Alexandridis,[†,‡] and Per Linse*[,†]

Physical Chemistry 1, Center for Chemistry and Chemical Engineering, Lund University, P.O. Box 124, S-221 00 Lund, Sweden, and Department of Chemical Engineering, State University of New York at Buffalo, Buffalo, New York 14260-4200

Received January 20, 1999; Revised Manuscript Received May 27, 1999

ABSTRACT: Ternary poly(ethylene oxide)−poly(propylene oxide)−poly(ethylene oxide) (PEO−PPO−PEO)/water/oil systems have been studied theoretically with a lattice mean-field theory. Phase diagrams for three PEO−PPO−PEO block copolymers are presented, and the existence of the ordered cubic micellar, hexagonal, lamellar, reverse hexagonal, and reverse cubic micellar phases as well as disorded water-rich and water-poor phases was considered. It was found that the length of the EO blocks strongly affected the phase behavior. The lamellar phase was studied in more detail with respect to the domain spacing and interfacial area per PEO block at different compositions and to the polymer conformations. The degree of looplike conformations and of bridging conformations across the apolar domain (PO + oil) was found to be dependent on the apolar domain thickness. Comparison with experimentally determined phase diagrams and lamellar domain spacings was also made.

Introduction

The interest in the self-assembly of poly(ethylene oxide)−poly(propylene oxide)−poly(ethylene oxide) (PEO−PPO−PEO) block copolymers has grown considerably over the past decade.[1−4] Triblock copolymers with the composition PEO−PPO−PEO, where PEO and PPO are poly(ethylene oxide) and poly(propylene oxide), respectively, is a group of polymers (commercially available as Pluronic or Synperonic) which displays amphiphilic behavior. Self-assembly of these polymers is facilitated, as in the case of common low-molecular-weight surfactants, by the presence of the two (or more) different but covalently bonded parts.

The solution properties of the PEO−PPO−PEO copolymers depend strongly on the interaction of the polymer segments with the solvent. The PPO middle block is more hydrophobic than the PEO end ones. Both types of blocks become more hydrophobic at increasing temperature, and at 25 °C and higher PPO is for all practical purposes hydrophobic. Therefore, in aqueous solutions, the PEO−PPO−PEO block copolymers self-associate into micellar-like aggregates with a core dominated by PO segments surrounded by water-swollen PEO blocks.[1,3,5] At a fixed temperature, the concentration at which the first micelles start to form is referred to as the critical micellization concentration (cmc). Another way to induce self-assembly, of particular interest in PEO−PPO−PEO block copolymers, is to increase the temperature. The temperature at which the micelles begin to form, now at a fixed concentration of the block copolymer, is referred to as the critical micellization temperature (cmt). The micelle formation of PEO−PPO−PEO in solution has also been studied theoretically,[6−12] and it is reasonably well-understood.

In addition to micelles in solution, these block copolymer form ordered lyotropic liquid crystalline (LLC) phases, similarly to low-molecular-weight surfactants and to block copolymer melts. Experimental phase behavior studies for a number of binary (PEO−PPO−PEO/water)[13−15] as well and ternary (PEO−PPO−PEO/water/oil)[2,16−22] systems have been presented, and structures such as cubic, hexagonal, and lamellar have been found. The phase behavior in these systems is indeed very rich; e.g., the Pluronic P84/water/xylene system displays nine different phases, all stable at the same temperature (25 °C) at different polymer/water/oil compositions.[21]

Whereas the experimental work on the ternary phase behavior for these systems has reached a level of maturity, the theoretical/modeling work on LLC phases in ternary systems in such systems is still limited. The transition from spherical to rodlike micelles at increased temperature in dilute aqueous solution of PEO−PPO−PEO has been studied with a lattice mean-field theory.[23] Later, the predictions of cubic, hexagonal, lamellar, reverse hexagonal, and reverse cubic phases at different temperatures were made, and phase diagrams were constructed for different PEO−PPO−PEO polymers of different molecular weight and EO/PO compositions using lattice and continuum mean-field theory.[24] In a subsequent paper,[25] we employed the same lattice approach[24] to further examine binary PEO−PPO−PEO/water systems. In particular, we determined the two-phase regions between the one-phase regions by applying the common tangent construction. The self-association of diblock cooligomers in ternary systems has also been examined using Monte Carlo simulation methods. Such studies have, for example, been performed by Larson for modeling surfactant/water/oil systems.[26] Larson found good agreement with experimentally determined binary phase diagrams, while a refinement of the model seems necessary to reproduce the experimental phase behavior in the ternary systems.

A related area is the phase behavior of ternary block copolymer AB/homopolymer A/homopolymer B systems. Recently, Janert and Schick[27] predicted from a continuum mean-field theory phase diagrams for blends of a diblock copolymer AB with homopolymers A and B. They found that homopolymers with a comparable

[†] Lund University.
[‡] State University of New York at Buffalo.

10.1021/ma990075r CCC: $18.00
Published on Web 07/09/1999

length to the diblock copolymer swelled the microstructure to a large extent, while addition of very short homopolymers induced disordered solution, attributed to a higher mixing entropy for these shorter homopolymers.

In this work, we have studied the ternary PEO−PPO−PEO/water/xylene system using the same lattice mean-field theory as in our previous work.[25] The cubic, hexagonal, lamellar, reverse hexagonal, and reverse cubic phases were considered, and their stabilities based on calculated free energy data were used to construct ternary phase diagrams. A more detailed study was performed on the lamellar phase for one of the systems, and predicted repeating distances were compared with experimental results obtained from small-angle X-ray scattering (SAXS). Finally, we have also examined the chain conformations of the block copolymers in the lamellar phase.

To the best of our knowledge, this work is the first one where ternary phase diagrams of block copolymer/solvent A/solvent B systems with a number of different ordered phases is modeled using mean-field theory. Moreover, the modeling is performed by employing realistic interaction parameters, and explicit comparison with experimental data is made.

Theoretical Model

Lattice Theory. A lattice mean-field theory was used to calculate the free energy of different ordered phases of ternary block copolymer/water/oil solutions, and thereafter phase diagrams were constructed on the basis of the relative free energies of the phases. The calculations were based on an extension of the Flory−Huggins lattice theory[28,29] to heterogeneous systems originally developed by Scheutjens and Fleer[30] and to polymers possessing internal degrees of freedom as developed by Karlström.[31]

The use of internal degrees of freedom provides a framework to describe the decreased solubility of EO- and PO-containing polymers in water with increasing temperature by employing physical arguments. Briefly, two conformational states, one polar and one apolar, are assigned to both the EO and PO segments. The apolar state is characterized with a higher internal energy and a higher statistical weight. Hence, the population of the apolar state is favored at an increasing temperature, whereas the polar state is favored at a reduced temperature. This results in more unfavorable polymer−water interaction upon a temperature increase. This approach has successfully rationalized a number of different properties of different systems composed by EO- and/or PO-containing polymers in aqueous solution.[8,11,12,24,31−35]

The extension of the Flory−Huggins theory to heterogeneous systems makes it possible to introduce and predict segment density profiles. Briefly, this is achieved by dividing the space between two reflective and planar surfaces (if planar geometry) or within a reflective and curved (if spherical or cylindrical geometry) surface into M layers. The layers are numbered $i = 1, 2, ..., M$, starting from the midpoint of the two planar surfaces or from the center of the curved surface, respectively, and each layer has L_i sites. The random (mean-field) mixing is applied within each layer separately.

The Helmholtz free energy of mixing, A, for a multicomponent system consisting of solvent(s) and polymer(s) with internal states can be expressed as[32]

$$\beta(A - A^*) = \beta(A_{\text{int}} - A_{\text{int}}^*) - \ln\frac{\Omega}{\Omega^*} + \beta(U - U^*) \quad (1)$$

where A_{int} and U represent the internal free energy and the configurational energy in the mixed system, respectively, while $\ln(\Omega/\Omega^*)$ is the mixing conformational entropy divided by the Boltzmann constant, and $\beta = 1/(kT)$, k being the Boltzmann constant and T the absolute temperature. Starred quantities denote corresponding quantities in a reference system where the components are in pure amorphous states. The internal free energy arising from the internal states becomes[32]

$$\beta A_{\text{int}} = \sum_i \sum_{\text{A}} n_{\text{A}i} \sum_{\text{B}} P_{\text{AB}i}\left[\beta U_{\text{AB}} + \ln\frac{P_{\text{AB}i}}{g_{\text{AB}}}\right] \quad (2)$$

where $\sum_i$ is the sum over layers, $n_{\text{A}i}$ is the number of sites in layer i occupied by segments of type A, and $P_{\text{AB}i}$ is the fraction of species A in layer i which is in state B (given by eq 6 in ref 32). Moreover, U_{AB} is the zero energy level of species A (either EO, PO, water, or xylene) in state B, and g_{AB} is the degeneration of species A in state B. In the case of EO (or PO), U_{AB} and g_{AB} describe the equilibrium between the polar and the apolar states of EO (or PO). The mixing entropy is given by[32]

$$\ln\frac{\Omega}{\Omega^*} = -\sum_x \sum_c n_{xc} \ln\frac{n_{xc} r_x}{\omega_{xc}} \quad (3)$$

where n_{xc} denotes the number of chains of component x in conformation c, r_x is the total number of segments in component x, and ω_{xc} is related to the degeneration factor for component x in configuration c, which is given by eq A.1.2 in ref 32.

The total interaction energy between the different states is expressed as[32]

$$\beta U = \frac{1}{2}\sum_{i=1}^{M} L_i \sum_{\text{A}} \sum_{\text{A}'} \sum_{\text{B}} \sum_{\text{B}'} \phi_{\text{A}i} P_{\text{AB}i} \chi_{\text{BB}'} \langle P_{\text{A}'\text{B}'i} \phi_{\text{A}'i} \rangle \quad (4)$$

where A and A′ run over all species and B and B′ over all states. $\phi_{\text{A}i}$ is the volume fraction of species A in layer i, and $\chi_{\text{BB}'}$ is the Flory−Huggins interaction parameter between species A in state B and species A′ in state B′. In the case of nearest-neighbor interactions, as applied here, $\langle ... \rangle$ indicates an average over the present and the two adjacent layers. From eqs 2−4 we may finally derive a species and spatial dependent potential $u_{\text{A}i}$ (given by eq 9 in ref 32), which depends on $\{\phi_{\text{A}i}\}$.

To close the set of equations, we need to express the volume fraction profiles $\{\phi_{\text{A}i}\}$ in terms of the potentials $\{u_{\text{A}i}\}$. Such a relation can be derived on the basis of Boltzmann-weighted conformations, conserved chain connectivity across the layer boundaries, and fulfilled packing constraint. (We again refer the reader to ref 32 for all the details.) Hence, at this stage we now possess an implicit set of nonlinear equations for the segment distributions, which can be solved numerically.

The extension of the above theory for calculation of the free energy and the relative stability of ordered LLC phases in binary systems was given by Noolandi et al.[24] We have here adopted the same approach, except for a slight modification due to the presence of one additional component. Five LLC ordered phases, viz. normal (oil-in-water) micellar cubic (I_1), normal hexagonal (H_1),

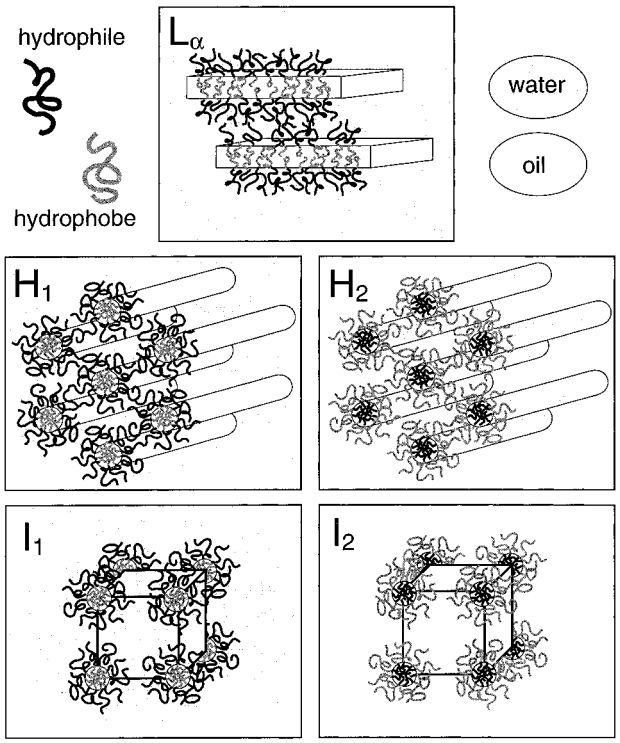

Figure 1. Schematic illustration of different modes of self-organization of a diblock copolymer in the presence of solvents ("water" and "oil") selective for each block. The block copolymers are localized at the interfaces between the polar ("water") and apolar ("oil") domains. For reasons of clarity, only the copolymer molecules at the cross section of the (spherical, cylindrical, and planar) assemblies are depicted, and only sections of the microstructures are shown. I_1, H_1, L_α, H_2, and I_2, denote normal (oil-in-water) micellar cubic, normal hexagonal, lamellar, reverse (water-in-oil) hexagonal, and reverse micellar cubic lyotropic liquid crystalline phases, respectively. The notation I, H, and L_α for the micellar cubic, hexagonal, and lamellar phase, respectively, is common in the surfactant literature, whereas in the block copolymer literature, the notation S, C, and L, respectively, often is used.

lamellar (L_α), reverse (water-in-oil) hexagonal (H_2), and the reverse micellar cubic (I_2) phase, were considered, and the structures of these phases are schematically given in Figure 1. Free energy curves for each phase were calculated by the following procedure. For a fixed block copolymer concentration, the $\phi_{water}/\phi_{xylene}$ ratio was decreased, and for each $\phi_{water}/\phi_{xylene}$ value the free energy of was minimized with respect to M. Such free energy curves were then repeatedly calculated for a set of specific $\phi_{polymer}$ with an interval of 0.05. By considering the free energy curves as a function of ϕ_{xylene} at fixed $\phi_{polymer}$ for the different ordered phases, the phase boundaries from the crossings of the free energy curves were obtained for the ordered phases. An illustration of this procedure is shown in Figure 2. No attempts to extract two- or three-phase regions from the free energy data were performed, and the possible presence of micellar in the disordered solutions was not accounted for in this study.

Polymer Model. We have performed model calculations of different PEO−PPO−PEO/water/xylene systems. Results will be given for (i) the $(EO)_{27}(PO)_{61}(EO)_{27}$ block copolymer (nominal structure for Pluronic P104) [experimental phase diagram and SAXS data of the lamellar phase are available for the ternary Pluronic P104/water/*p*-xylene system[20]], (ii) the $(EO)_{50}(PO)_{61}(EO)_{50}$ block copolymer, and (iii) the $(EO)_{107}(PO)_{61}(EO)_{107}$ block copolymer. All copolymers have the same PPO block length, but the size of the PEO blocks differs. Unless otherwise noted, all calculations were performed at $T = 298$ K.

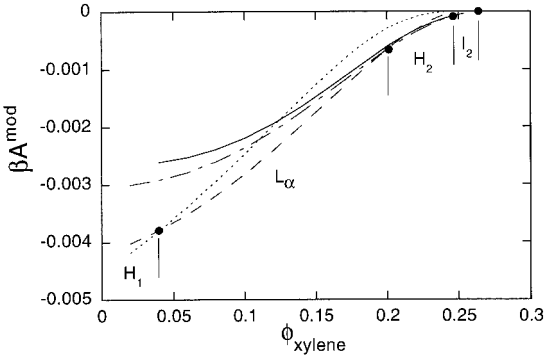

Figure 2. Reduced modified free energy (βA^{mod}) of the normal hexagonal H_1 (dotted curve), lamellar L_α (dashed curve), reverse hexagonal H_2 (dot−dashed curve), and reverse cubic I_2 phase (solid curve) versus volume fraction of xylene (ϕ_{xylene}) for the $(EO)_{27}(PO)_{61}(EO)_{27}$/water/xylene system at $\phi_{polymer} = 0.45$. $A^{mod} = A - A^{hom}$, where A is the free energy given by eq 1 and A^{hom} is free energy of the corresponding homogeneous (disordered) system. The subtraction with A^{hom} facilitates the visualization of the free energy crossings (filled spheres) by reducing the slope of the free energy curves without affecting the locations of the crossings.

Table 1. Internal State Parameters (U_{AB} and g_{AB}) and Flory−Huggins Interaction Parameters ($\chi_{BB'}$) of the Theoretical Model (Energy in kJ mol^{-1})

species	state	U_{AB}	g_{AB}
water		0	1
EO	polar	0[a]	1[a]
EO	apolar	5.086[a]	8[a]
PO	polar	0[b]	1[b]
PO	apolar	11.5[b]	60[b]
xylene		0	1

	$RT\chi_{BB'}$				
state	EO_{polar}	EO_{apolar}	PO_{polar}	PO_{apolar}	xylene
water	0.6508[a]	5.568[a]	1.7[b]	8.5[b]	6.3[d]
EO_{polar}		1.266[a]	1.8[c]	3.0[c]	1.81[d]
EO_{apolar}			0.5[c]	−2.0[c]	1.81[d]
PO_{polar}				1.4[b]	1.48[d]
PO_{apolar}					1.48[d]

[a] From the fit to the experimental PEO/water phase diagram.[31] [b] From the fit to the experimental PPO/water phase diagram.[32] [c] From the fit to the experimental PEO/PPO/water phase diagram.[33] [d] Determined in this work.

Parameter Evaluation. The values of the parameters U_{AB}, g_{AB}, and $\chi_{BB'}$ used are listed in Table 1. Except for parameters related to xylene, all other were taken from previous investigations (see Table 1). The interaction between xylene and water is repulsive, and we have used $RT\chi_{water,xylene} = 6.3$ kJ mol^{-1}, which could be compared with 5.5 kJ mol^{-1} as used for the benzene−water interaction in a study of benzene solubilization in PEO−PPO−PEO micellar solutions by Hurter et al.[10] An increase of $\chi_{water,xylene}$ by ∼25% resulted in an unrealistic phase diagram, and a corresponding decrease in only a small change of the phase boundaries.

To obtain the interaction parameters between xylene and the different polymer species (EO and PO), PEO homopolymer and PPO homopolymer were separately dissolved in *o*-xylene to approximately 10 wt % polymer, and the temperature for phase separation was determined. Calculations based on the Flory−Huggins lattice

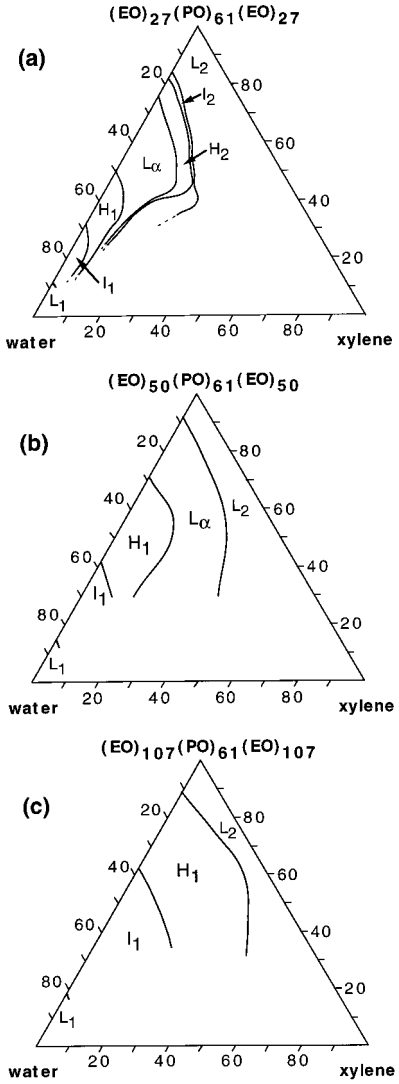

Figure 3. Ternary phase diagrams of (a) the $(EO)_{27}(PO)_{61}(EO)_{27}$/water/xylene system, (b) the $(EO)_{50}(PO)_{61}(EO)_{50}$/water/xylene, and (c) the $(EO)_{107}(PO)_{61}(EO)_{107}$/water/xylene system. The notations are explained in the text, and the concentrations are expressed in volume percent.

theory were performed, and the χ value between the polymer (PEO or PPO) and xylene was adjusted until phase separation occurred at the experimentally determined temperature (20 and −26 °C for PEO and PPO, respectively). For both EO and PO, their two states were assumed to have the same interaction with xylene. More experimental data are needed to make a more elaborate fit.

Results and Discussion

Ternary Phase Diagrams. The predicted ternary phase diagram for the $(EO)_{27}(PO)_{61}(EO)_{27}$/water/xylene system is shown in Figure 3a. Several different ordered phases as well as water-rich and water-poor disordered phases were obtained, and as mentioned above (see Figure 2), the phase boundaries were determined from the crossings of the free energy curves. Five ordered phases were stable along the binary PEO−PPO−PEO/water axis, while the model predicts no ordered structure to be stable along the PEO−PPO−PEO/xylene axis. Starting at the water corner and proceeding along the PEO−PPO−PEO/water axis toward the block copolymer corner, the following sequence of phases was observed: disordered water-rich (L_1), normal micellar cubic (I_1), normal hexagonal (H_1), lamellar (L_α), reverse hexagonal (H_2), the reverse micellar cubic (I_2), and disordered water-poor (L_2) phase. The lamellar phase is the most extensive one, and it is stable in the range $\phi_{water} = 0.25-0.50$.

The LLC phases appearing along the PEO−PPO−PEO/water axis accommodate xylene to different degrees. The amount of xylene possible to accommodate increases from the I_1 phase to the I_2 phase. The normal phases I_1 and H_1 are stable up to $\phi_{xylene} \approx 0.1$, whereas the lamellar phase may contain up to ca. 20 vol % xylene. The reverse phases H_2 and I_2 tend to encircle the other phases, and I_2 can accommodate most xylene of the phases, 30 vol % xylene at $\phi_{polymer} = 0.4$. It is thus clearly observed that an addition of oil at a given PEO−PPO−PEO/water ratio favors the stability of phases that curve less toward oil and more toward water.

The effect on the phase behavior of extending the PEO block length is strong. Parts b and c of Figure 3 show the phase diagrams for the $(EO)_{50}(PO)_{61}(EO)_{50}$/water/xylene and the $(EO)_{107}(PO)_{61}(EO)_{107}$/water/xylene systems, respectively. As the PEO block length increases, the normal ordered phases are favored. The $(EO)_{50}(PO)_{61}(EO)_{50}$/water/xylene phase diagram (Figure 3b) contains the ordered phases: normal micellar cubic (I_1), normal hexagonal (H_1), and the lamellar (L_α) phases, whereas in the binary $(EO)_{107}(PO)_{61}(EO)_{107}$/water system, the only ordered phases remaining are the I_1 and H_1 phases (Figure 3c). Moreover, Figure 3c shows that these phases may swell considerably by the addition of oil. Hence, the swelling capacity of a given ordered phase increases as the hydrophilic PEO block length increases at constant hydrophobic PPO block length.

In addition to the phase diagrams given in Figure 3, ternary phase diagrams of $(EO)_{30}(PO)_{69}(EO)_{30}$ and $(EO)_{68}(PO)_{69}(EO)_{68}$ were also determined (results not shown). The $(EO)_{30}(PO)_{69}(EO)_{30}$/water/xylene system exhibited a nearly identical phase diagram as for the $(EO)_{27}(PO)_{61}(EO)_{27}$/water/xylene system, whereas the $(EO)_{68}(PO)_{69}(EO)_{68}$/water/xylene system displayed a phase diagram similar to that of the $(EO)_{50}(PO)_{61}(EO)_{50}$/water/xylene system. These findings demonstrate that a 10% change in the molecular weight, given a nearly constant EO/PO ratio, does not give rise to a noticeable difference in the stability regions of the different ordered microstructures, in agreement with experimental results (e.g., cf. phase diagrams of Pluronic 84/water/xylene[21] and Pluronic 104/water/xylene[20]).

We will now compare the predicted phase diagrams with experimental data. Starting with the $(EO)_{27}(PO)_{61}(EO)_{27}$/water/xylene system, a comparison of the predicted phase diagram given in Figure 3a with the experimentally determined one by Svensson et al.[20] shows that (i) the experimentally observed sequence of micellar cubic, hexagonal, lamellar, reverse hexagonal, and reverse micellar cubic ordered phases is reproduced by the model, (ii) the lamellar region is found to be the most extensive one in both the experiment and the model, (iii) the prediction that no structure is stable along the polymer/oil axis agrees with the experiment, and (iv) the transition to lower curvature from micellar cubic, to hexagonal, to lamellar, to reverse hexagonal, and to reverse micellar cubic, predicted when oil is replacing water at a constant polymer concentration, is also observed in the experiments. The main disagreement is the prediction of the location and extension of

the reversed hexagonal and reversed cubic phases. Experimentally, they are not stable without addition of at least 20% and 40% oil, respectively, and their extensions are considerably larger than those predicted by the model.

The predicted preference of high-curvature oil-in-water micellar cubic and hexagonal structures upon increasing PEO block lengths at constant PPO block length is in agreement with experimental data. For example, the ternary phase diagrams for Pluronic P123/water/butyl acetate and Pluronic F127/water/butyl acetate displayed a similar extension of the I_1 and H_1 phases when the number of EO segments in the PEO blocks was increased from 20 to 100. This effect can be understood from simple geometrical reasons. As the polar PEO block increases in length, keeping the size of the hydrophobic PPO block constant, the volume of the corona composed of hydrated PEO chains increases, leading to a stabilization of structures with higher curvature toward oil.

Hence, the model can predict a number of characteristic features of PEO−PPO−PEO/water/oil systems. Along the PEO−PPO−PEO/water axis the predictions are semiquantitative (see also refs 24 and 25), whereas the predictions are less accurate on the water-lean side of the ternary phase diagram (e.g., along the polymer/oil axis). For example, for the $(EO)_{27}(PO)_{61}(EO)_{27}$/water/xylene system, the experimental phase diagram is more symmetric around the $\phi_{water}/\phi_{xylene} = 1$ dilution line than predicted by the model. At present, we have no clear understanding of this discrepancy or whether this could be remedied by improved interaction parameters involving xylene or by allowing $\chi_{water,xylene}$ to depend on ϕ_{water} or whether more fundamental changes are needed.

Microstructure of the Lamellar Phase. Some predicted properties of the lamellar phase of the $(EO)_{27}(PO)_{61}(EO)_{27}$/water/xylene system will now be examined in more detail.

Volume Fraction Profiles. The numerical solutions involve a determination of the volume fraction profiles of the ordered LLC phases. We will here consider profiles for two different compositions of the lamellar phase. For a system laying on the PEO−PPO−PEO/water axis at $\phi_{polymer} = 0.55$ (see Figure 3a), Figure 4a shows that the PO species form an apolar domain (centered at $i = 0$), whereas the EO and water species are preferentially located outside the apolar domain; still, an appreciable water content in the apolar domain is predicted. Figure 4b shows the volume fraction profiles for the lamellar phase at the same $\phi_{polymer}$ as in Figure 4a, but with some water replaced by xylene, making the composition laying on the border to the H_2 phase. The shape of the profiles of EO, PO, and water species is generally the same as in the binary system, but the differences of the species concentrations between the polar and apolar domains are smaller. It is also seen that xylene is nearly evenly distributed throughout the system. Only a weak maximum in the apolar domain is predicted, which is an unexpected result and in contradiction with the common sense that xylene is located in the apolar domain. Although the xylene volume fraction profiles were monitored during the fitting of the xylene interaction parameters, a more uneven distribution was not possible to achieve while still maintaining a reasonable phase diagram.

Domain Spacing and Interfacial PEO Area. As alluded to in the "Theoretical Model" section, the calculation of the free energy for a given composition was accompanied by an optimization of the domain spacing. Figure 5 shows a contour plot of the obtained domain spacing and the phase boundary of the lamellar phase. It is clear that the domain spacing varies with the composition. The largest spacing was obtained at low block copolymer concentrations; at increasing block copolymer concentration the domain spacing decreased, a trend also found experimentally for the Pluronic P104/water/*p*-xylene system. (The experimental contour plot will be published in a later paper from this laboratory.[36]) The contour lines rotate from being parallel to the ϕ_{xylene} axis at low polymer concentration to being diagonal at

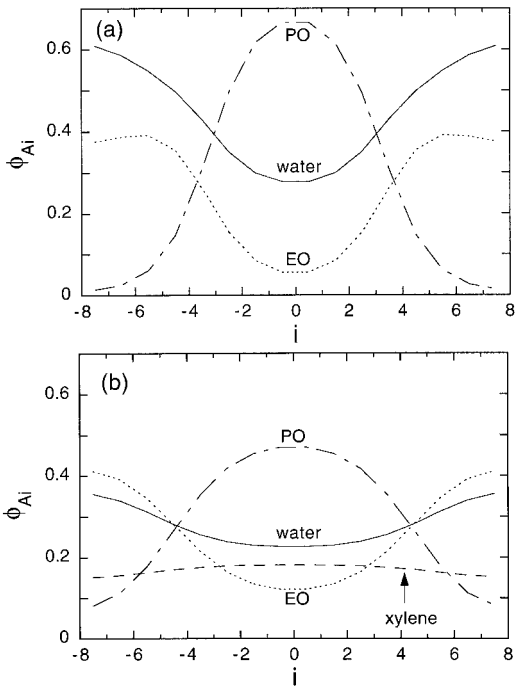

Figure 4. Species volume fraction (ϕ_{Ai}) versus layer number (i) for the lamellar phase of (a) the $(EO)_{27}(PO)_{61}(EO)_{27}$/water system at $\phi_{polymer} = 0.55$ and $\phi_{water} = 0.45$ and (b) the $(EO)_{27}(PO)_{61}(EO)_{27}$/water/xylene system at $\phi_{polymer} = 0.55$, $\phi_{water} = 0.28$, and $\phi_{xylene} = 0.17$.

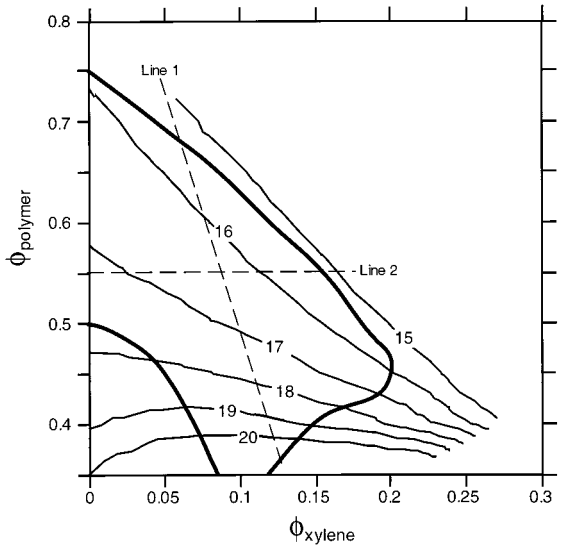

Figure 5. Contour plot of domain spacing (thin solid curves) and phase boundary of the lamellar phase (thick solid curves) of the $(EO)_{27}(PO)_{61}(EO)_{27}$/water/xylene system. Dilution lines corresponding to $\phi_{water}/\phi_{xylene} = 4$ (line 1) and $\phi_{polymer} = 0.55$ (line 2) are also given.

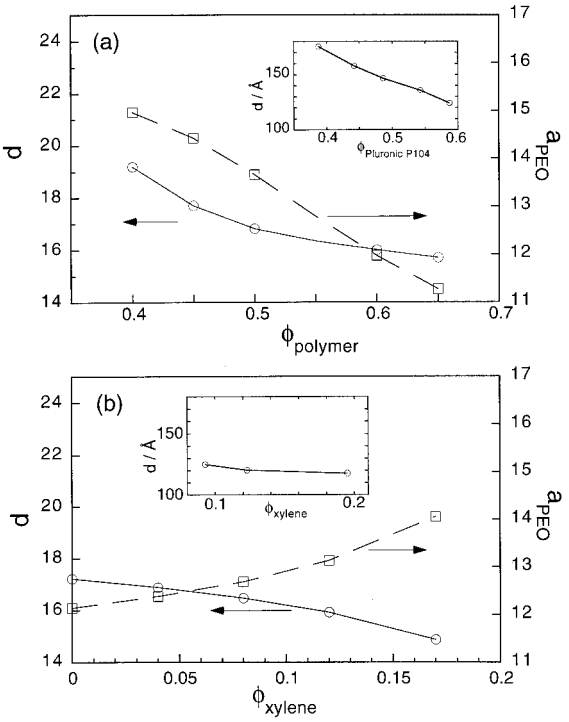

Figure 6. Domain spacing (d, circles) and interfacial area per PEO block (a_{PEO}, squares) versus (a) volume fraction of $(EO)_{27}(PO)_{61}(EO)_{27}$ (corresponding to line 1 in Figure 5) and (b) volume fraction of xylene (corresponding to line 2 in Figure 5). Experimental results for corresponding lines of the lamellar phase are given in the insets (data from ref 36).

higher polymer concentration. Experimentally, this rotation is very weak, and the contour lines stay nearly parallel to the ϕ_{xylene} axis throughout the whole lamellar phase.

To further investigate the lamellar phase, two dilution lines with different component ratios have been selected; these lines are indicated in Figure 5. Line 1 represents variable $\phi_{polymer}$ at solvent ratio $\phi_{water}/\phi_{xylene} = 4$ and line 2 variable solvent ratio at $\phi_{polymer} = 0.55$. Figure 6 shows the domain spacing and the interfacial area per PEO block $\{a_{PEO} = (r_{polymer}/2)[(d/2)\phi_{polymer}]\}$ of the lamellar phase as a function of a suitable concentration variable for the two dilution lines. The insets in Figure 6 show the experimentally determined domain spacing for fixed component ratios (which span the lamellar phase in similar manners as the lines in Figure 5) in the Pluronic P104/water/*p*-xylene system.

A comparison between the experimental and model results shows a qualitative agreement, i.e., a relatively large change in the domain spacing along line 1 and a smaller change along line 2. However, the model underestimates the relative reduction of the domain size of the lamellar phase at increasing $\phi_{polymer}$ along line 1, $[(15.7 - 19.2)/19.2 =] -0.18$ as compared to $[(124 - 175)/175 =] -0.29$ for the experimental data and overestimates the relative reduction at increasing ϕ_{xylene} along line 2 $[(14.9 - 17.2)/17.2 =] -0.13$ as compared to $[(118 - 125)/125 =] -0.06$. The latter discrepancy is of course related to the larger rotation of the contour curves (see Figure 5) at increasing $\phi_{polymer}$ obtained from the model. In previous contributions, where the micellization and adsorption to surfaces of Pluronic polymers have been modeled with the same theory, the assignment of 4 Å to the lattice unit length has given acceptable to good agreement between experimental and model results.[8,34]

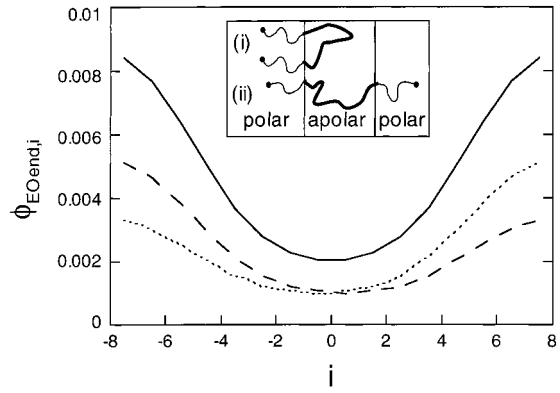

Figure 7. Volume fraction of EO end segments ($\phi_{EOend,i}$) versus layer number (i) for the lamellar phase (solid curve) and its division into the conditional cases that the other end segment is located at $i < 0$ (dashed curve) and $i > 0$ (dotted curve) for the $(EO)_{27}(PO)_{61}(EO)_{27}$/water/xylene system at $\phi_{polymer} = 0.55$, $\phi_{water} = 0.28$, and $\phi_{xylene} = 0.17$. The classification into (i) looplike and (ii) bridging conformations is illustrated in the inset.

However, the same choice would here lead to a discrepancy in the domain spacing by a factor of 2. Besides the effects of the shortcoming of the simple lattice model, the effect of polymer length polydispersity in the experimental samples contributes to this discrepancy. Previously, we predicted that a length polydispersity gives rise to an extended spacing in the lamellar phase.[25]

Figure 6a also shows that the interfacial area per PEO block is predicted to decrease with increasing $\phi_{polymer}$ at fixed $\phi_{water}/\phi_{xylene}$ ratio. The substitution of water and xylene with equal amount of block copolymer leads to less swollen polymers, which in turn both reduces the area for the block copolymers at the interface and the longitudinal extension of the polymer. On the other side, the increase in ϕ_{xylene} and a concomitant reduction of ϕ_{water} leads to the mentioned reduction of the lamellar spacing, but now the area per PEO block is predicted to increase. The opposite trends of d and a_{PEO} is expected here, since the product of d and a_{PEO} is for geometrical reasons constant at fixed $\phi_{polymer}$, given that the flux of polymers passing the interface is not altered and the lamellar phase is preserved.

Chain Conformations. In addition to the volume fraction profiles of a given species, the theory allows extraction of the volume fraction profiles of any given segment; i.e., the density profile can be determined for any specified segment in the polymer chain. We have chosen to investigate the volume fraction profiles of the (EO) end segments of the triblock copolymer. Moreover, the locations of these segments have been used to divide the block copolymers in the lamellar phase into two classes according to the conformation of the copolymer.

Figure 7 shows the density profile of the end segments of the copolymers for the $(EO)_{27}(PO)_{61}(EO)_{27}$/water/xylene system (solid curve). It is seen that the largest probability of finding the end segments is in the polar domain, consistent with the EO/PO segregation shown in Figure 4b. The ca. 25-fold reduction in the volume fraction of $\phi_{EOend,i}$, as compared to $\phi_{EO,i}$, is related to the fact that there is one EO end segment per 27 EO segments.

By specifying that the other end segment, which is residing in the other PEO block of the polymer, is

localized at one of the two sides of the middle of the apolar domain, conditional volume fraction profiles for a given end segment can be obtained. Figure 7 also shows such end segment volume fraction profiles given that the other one is either at $i < 0$ (dashed curve) or $i > 0$ (dotted curve). The two conditional profiles provides a detailed picture of the probability of finding an end segment at a given location given that the other is located at either side of the center of the apolar domain. The difference between the conditional profiles shows that a looplike conformation (with both end segments located at the same side with respect to the middle of apolar domain) is more likely than a bridging one (with the polymer spanning through the apolar domain so that the two end segments are located on each side of the apolar domain) (see inset of Figure 7). However, the difference is not pronounced. We believe that a larger excess of looplike conformations is inconsistent with a stable lamella formed by flexible polymers. Similar investigations, but for the PEO−PPO junctions, for binary PEO−PPO−PEO/water systems have been presented previously, and those results[24] are consistent with these in Figure 7.

We now proceed by defining the fraction of looplike conformations according to

$$f_{\text{loop}} = \frac{\sum_{i<0} \phi'_{\text{EOend},i}}{\sum_{i} \phi'_{\text{EOend},i}} \qquad (5)$$

where $\phi'_{\text{EOend},i}$ is the conditional volume fraction of end segments in layer i given that the other end segment is located at $i < 0$.[37] A higher value of f_{loop} indicates more looplike conformations of the block copolymer chains. In our systems, we always have $f_{\text{loop}} > 0.5$, and we do neither expect $f_{\text{loop}} < 0.5$ since the chains are completely flexible and direct back-folding of them is permitted. However, for stiffer chains,[38] $f_{\text{loop}} < 0.5$ would be possible.

We anticipate that the fraction of loops is related to the apolar domain thickness. An increased thickness of the apolar domain would make it less likely for the triblock copolymer to span the apolar domain, and hence, an increased probability to find both end segments on the same side of the apolar domain is reasonable. This was investigated by calculation of the fraction of loops along the composition lines given in Figure 5. Figure 8 shows the result together with the domain spacing and the thickness of the apolar domain. The latter was evaluated as the width of the apolar domain at the half-height of the highest volume fraction of PO.[37] Since both f_{loop} and d_{apolar} increases with increasing ϕ_{polymer} (Figure 8a) and $\phi_{\text{water}}/\phi_{\text{xylene}}$ (Figure 8b), the notion of an increased f_{loop} with increasing d_{apolar} is supported.

The domain spacing and the thickness of the apolar domain of the lamellae may also be varied by changing the temperature at a fixed composition. A temperature increase results in a decrease in solubility of PEO and PPO in water, leading to less hydrated PEO blocks and consequently to a smaller interfacial area in the lamellar phase.[15,24] This effect was employed for the binary $(EO)_{27}(PO)_{61}(EO)_{27}$/water system. In Figure 9, the domain spacing, the thickness of the apolar domain, and the fraction of loops are given as a function of the

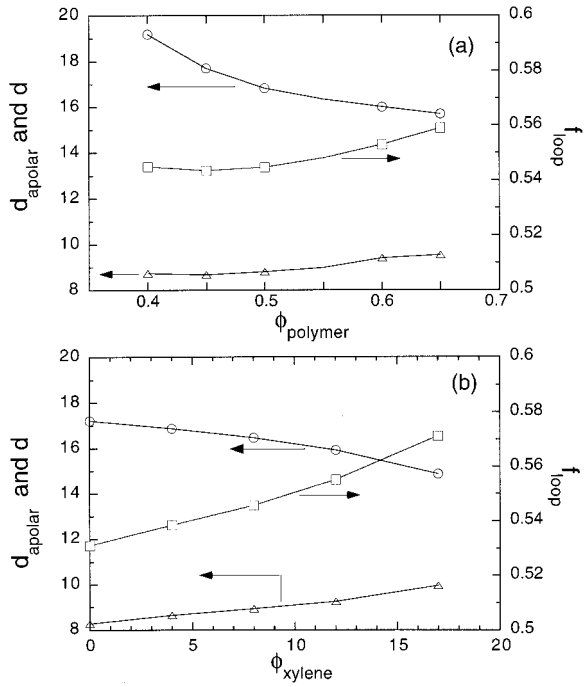

Figure 8. Domain spacings (d, circles), apolar domain thickness (d_{apolar}, squares), and fraction of loops (f_{loop}, triangles) versus (a) volume fraction of $(EO)_{27}(PO)_{61}(EO)_{27}$ (corresponding to line 1 in Figure 5) and (b) volume fraction of xylene (corresponding to line 2 in Figure 5).

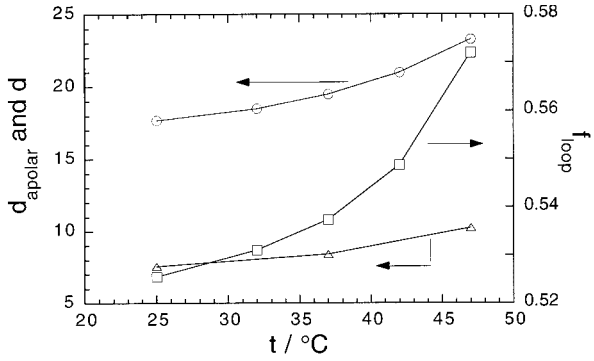

Figure 9. Domain spacings (d, circles), apolar domain thickness (d_{apolar}, squares), and fraction of loops (f_{loop}, triangles) versus temperature (t) of the lamellar phase of the binary $(EO)_{27}(PO)_{61}(EO)_{27}$/water system at $\phi_{\text{polymer}} = \phi_{\text{water}} = 0.5$.

temperature. As seen in Figure 9, both f_{loop} and d_{apolar} increase with increasing temperature, resulting in the same qualitative relation between f_{loop} and d_{apolar} as above.

Moreover, Figures 8 and 9 also display the variation of the domain spacing. In Figure 8, d and f_{loop} are negatively correlated, whereas in Figure 9 they are positively correlated; thus, d seems not to be primarily correlated with f_{loop}.

Finally, to examine the strength of the dependency of the fraction of loops on the thickness of the apolar domain, Figure 10 displays f_{loop} as a function of d_{apolar} using all the data displayed in Figures 8 (concentration variation) and 9 (temperature variation). Since the data in Figure 10 essentially collapse on a master curve, the fraction of loops of the block copolymers seems solely dependent on the magnitude of d_{apolar} and not on how the change of d_{apolar} is achieved.

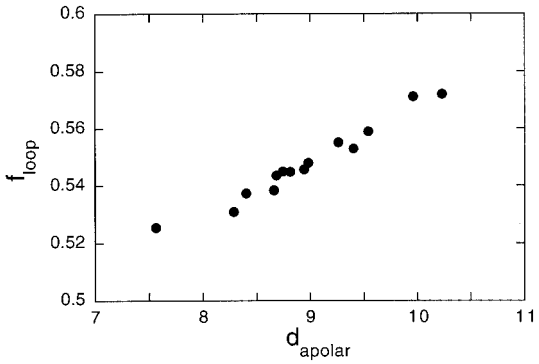

Figure 10. Fraction of loops (f_{loop}) versus corresponding apolar domain thickness (d_{apolar}) for the data shown in Figures 8 and 9.

Conclusions

This work reports on theoretical predictions of the phase behavior in ternary PEO−PPO−PEO/water/xylene systems. We have used a lattice model extended with internal degrees of freedom for the EO and the PO segments to account for the temperature-dependent solubility of the species in the block copolymer. The calculations involved free energy determination of the following ordered phases: normal micellar cubic (I_1), normal hexagonal (H_1), lamellar (L_α), reverse hexagonal (H_2), and the reverse micellar cubic (I_2). The boundaries between one-phase regions in the ternary phase diagrams were determined by the relative stability of the ordered phase given by the magnitude of the free energy. The predicted ternary phase diagrams for $(EO)_{27}(PO)_{61}(EO)_{27}$/water/xylene, $(EO)_{50}(PO)_{61}(EO)_{50}$/water/xylene, and $(EO)_{107}(PO)_{61}(EO)_{107}$/water/xylene were presented. In the phase diagram of $(EO)_{27}(PO)_{61}(EO)_{27}$, all the five different ordered phases were found stable. With increasing length of the PEO blocks the reverse phases become unstable, and for the $(EO)_{50}(PO)_{61}(EO)_{50}$ polymer, the remaining ordered phases are the normal cubic, the normal hexagonal, and the lamellar phase. For the polymer with the longest PEO blocks, $(EO)_{107}$-$(PO)_{61}(EO)_{107}$, only the I_1 and H_1 phases are the remaining ordered phases. This difference in the phase behavior is the expected one from the variation of the size of the water-soluble PEO block. An increase in size of the PEO block favors structures with curvature toward the apolar domain (normal structures) in the microstructure.

The lamellar phase of the $(EO)_{27}(PO)_{61}(EO)_{27}$/water/xylene system was studied in more detail. The domain spacing (repeating distance), the interfacial area for the block copolymer, and the size of the apolar domain were monitored along two dilution lines in the lamellar phase. The trends in domain spacing were in qualitative agreement with experimental findings for the same ternary system.

We finally examined the frequency of two classes of conformations that the block copolymer may adopt in the lamellar phase, viz., a looplike conformation and a bridging stretch−trough conformation, based on the volume fraction profiles for the end segments of the block copolymer. The looplike conformation was more probable, but its dominance was small. A direct dependence between the fraction of looplike conformations and the thickness of the apolar domain (the PPO-rich domain), was established. A larger size of the apolar domain increased the fraction of looplike conformations.

Generally the predicted properties are in agreement with experimental data, although the model has difficulties in predicting the location and extension of the reverse phases. However, the qualitative agreement of the predicted phase behavior and variation in the lamellar domain spacing with experiments confer confidence to the model predictions of other properties as the segment density profiles and the end-block distribution. Hence, the predictive ability developed in this study should be useful in practical applications of PEO−PPO−PEO block copolymers, and the detailed structural information obtained from the model is important for our understanding of the conformations of block copolymers in solvents. Such detailed structural information is not yet accessible from experiments.

Acknowledgment. We thank Birgitta Svensson for providing experimental SAXS data prior to publication and for fruitful discussions. This work was supported financially by the Swedish Research Council for Engineering Sciences (TFR) and the Swedish National Research Council (NFR). P.A. acknowledges the donors of the Petroleum Research Fund, administered by the American Chemical Society, for partial support of this research.

References and Notes

(1) Alexandridis, P.; Hatton, T. A. *Colloids Surf. A* **1995**, *96*, 1.
(2) Alexandridis, P.; Olsson, U.; Lindman, B. *Macromolecules* **1995**, *28*, 7700.
(3) Chu, B.; Zhou, Z. In *Nonionic Surfactants: Polyoxyalkylene Block Copolymers*; Nace, V. M., Ed.; Marcel Dekker: New York, 1996; Vol. 60, p 67.
(4) Alexandridis, P. *Curr. Opin. Colloid Interface Sci.* **1997**, *2*, 478.
(5) Almgren, M.; Brown, W.; Hvidt, S. *Colloid Polym. Sci.* **1995**, *273*, 2.
(6) Nagarajan, R.; Ganesh, K. J. *J. Chem. Phys.* **1989**, *90*, 5843.
(7) Linse, P.; Malmsten, M. *Macromolecules* **1992**, *25*, 5434.
(8) Linse, P. *Macromolecules* **1993**, *26*, 4437.
(9) Hurter, P. N.; Scheutjens, J. M. H. M.; Hatton, T. A. *Macromolecules* **1993**, *26*, 5592.
(10) Hurter, P. N.; Scheutjens, J. M. H. M.; Hatton, T. A. *Macromolecules* **1993**, *26*, 5030.
(11) Linse, P. *Macromolecules* **1994**, *27*, 2685.
(12) Linse, P. *Macromolecules* **1994**, *27*, 6404.
(13) Wanka, G.; Hoffman, H.; Ulbricht, W. *Macromolecules* **1994**, *27*, 4145.
(14) Zhang, K.; Khan, A. *Macromolecules* **1995**, *28*, 3807.
(15) Alexandridis, P.; Zhou, D.; Khan, A. *Langmuir* **1996**, *12*, 2690.
(16) Holmqvist, P.; Alexandridis, P.; Lindman, B. *Macromolecules* **1997**, *30*, 6788.
(17) Alexandridis, P.; Holmqvist, P.; Lindman, B. *Colloids Surf. A* **1997**, *129−130*, 3.
(18) Caragheorgheopol, A.; Pilar, J.; Schlick, S. *Macromolecules* **1997**, *30*, 2923.
(19) Zhou, S. Q.; Su, J.; Chu, B. *J. Polym. Sci. B: Polym. Phys.* **1998**, *36*, 889.
(20) Svensson, B.; Alexandridis, P.; Olsson, U. *J. Phys. Chem. B* **1998**, *102*, 7541.
(21) Alexandridis, P.; Olsson, U.; Lindman, B. *Langmuir* **1998**, *14*, 2627.
(22) Holmqvist, P.; Alexandridis, P.; Lindman, B. *J. Phys. Chem. B* **1998**, *102*, 1149.
(23) Linse, P. *J. Phys. Chem.* **1993**, *97*, 13896.
(24) Noolandi, J.; Shi, A.-C.; Linse, P. *Macromolecules* **1996**, *29*, 5907.
(25) Svensson, M.; Alexandridis, P.; Linse, P. *Macromolecules* **1999**, *32*, 637.
(26) Larson, R. G. *J. Phys. II* **1996**, *6*, 1441.
(27) Janert, P. K.; Schick, M. *Macromolecules* **1997**, *30*, 137.
(28) Huggins, M. L. *J. Phys. Chem.* **1942**, *46*, 151.
(29) Flory, P. J. *J. Chem. Phys.* **1942**, *10*, 51.
(30) Fleer, G. J.; Cohen Stuart, M. A.; Scheutjens, J. M. H. M.; Cosgrove, T.; Vincent, B. *Polymers at Interfaces*; Chapman and Hall: New York, 1993.

(31) Karlström, G. *J. Phys. Chem.* **1985**, *89*, 4962.
(32) Linse, P.; Björling, M. *Macromolecules* **1991**, *24*, 6700.
(33) Malmsten, M.; Linse, P.; Zhang, K.-W. *Macromolecules* **1993**, *26*, 2905.
(34) Linse, P.; Hatton, T. A. *Langmuir* **1997**, *13*, 4066.
(35) Svensson, M.; Linse, P. *Macromolecules* **1998**, *31*, 1427.
(36) Svensson, B.; Olsson, U.; Alexandridis, P. Manuscript in preparation.
(37) When determining f_{loop} and d_{apolar} for a given composition with a accompanied optimized domain spacing d (which not necessarily has to be an integer), the two nearby integer domain spacings were used, and f_{loop} and d_{apolar} were determined by linear interpolation. This procedure were tested against a quadratric fit using data from three domain spacings which improved f_{loop} and d_{apolar} with at most 1%.
(38) Leermakers, F. A. M.; van der Schoot, P. P. A. M.; Schutjens, J. M. H. M.; Lyklema, J. In *Surfactants in Solution*; Mittal, K. L., Ed.; Plenum: New York, 1990; Vol. 7, p 25.

MA990075R